Vol 18 No 8, August 2009
1674-1056/2009/18(08)/3500-08

Chinese Physics B

© 2009 Chin. Phys. Soc.
and IOP Publishing Ltd

Influence of solute cloud and precipitates on spatiotemporal characteristics of Portevin-Le Chatelier effect in A2024 aluminum alloys*

Sun Liang(孙 亮), Zhang Qing-Chuan(张青川)†, and Cao Peng-Tao(曹鹏涛)

CAS Key Laboratory of Mechanical Behavior and Design of Materials, University of Science and Technology of China, Hefei 230027, China

(Received 12 October 2008; revised manuscript received 1 December 2008)

In this paper, solute concentration and precipitate content in A2024 aluminum alloy are adjusted by solution treatment (ST) at different temperatures and tensile experiments on these treated specimens are carried out. It is found that the temperature of solution treatment (ST temperature) has a remarkable influence on the amplitude of the serrated flow and the propagation characteristics of shear bands. These results are due to the effects of solute atoms and precipitates on dynamic strain aging (DSA). When ST temperature is higher than 300 °C, solute concentration is relatively high and solute cloud is a key factor of DSA. When ST temperature is lower than 300 °C, precipitate content is relatively high and the mechanism of DSA is determined by precipitates.

Keywords: aluminum alloy, Portevin-Le Chatelier effect, dynamic strain aging, solution treatment, precipitate particle

PACC: 6220F, 8140C

1. Introduction

The Portevin-Le Chatelier (PLC) effect,[1−3] which is characteristic of inhomogeneous deformation band and repeated stress serrations, has been observed in many alloys. This phenomenon, as one of the most prominent examples for plastic instabilities, occurs within a certain regime of temperatures and loading rates. Temporally the PLC effect is featured as serrated flow on stress-time curves and strain staircase on strain-time curves, and spatially as repeated initiation and propagation of shear bands. According to the dynamics of the nucleation and motion of PLC bands, three types of instabilities, i.e. types A, B and C, can be observed in alloys loaded at constant speed.[4−8]

During the last few decades, the PLC effect has been extensively studied and it is generally considered to be the consequence of dynamic interactions between gliding dislocations and mobile solute atoms[9−14] i.e., dynamic strain aging (DSA). But the micro-mechanism of DSA is still under discussion. Originally Cottrell and Bilby[9,15] assumed that solute atoms had a drift speed of the order of dislocation speed and could move together with dislocations. Later on, researchers like McCormick[16] and van den Beukel[11] found the mobility of solute atoms to be not so high. After a mobile dislocation has been impeded by obstacles such as forest dislocations, precipitates grain boundaries etc., a solute cloud forms around it through pipe diffusion[17,18] and glide dislocation is effectively pinned. With applied stress, obstacles can be conquered by thermally activated dislocation motion. The PLC effect is brought into being in response to dynamic repeated pinning and unpinning processes between mobile dislocations and solute atoms. Up to now two kinds of phenomenological models have been put forward, viz. dislocation kinetic model[19−22] in which the conversion of various dislocations is considered, and a solute kinetic model[14,23−27] in which the variation of solute concentration around glide dislocations is studied.

In the previous studies of our group, by digital speckle pattern interferometry (DSPI) and digital speckle correlation (DSC), the nucleation and the propagation of PLC band were visualized and quantitatively measured by fringe patterns and some novel evolution phenomena were investigated[28,29] A new constitutive model which is based on the dynamic in-

*Project supported by the National Natural Science Foundation of China (Grant Nos 10872189 and 10732080).

†To whom correspondence should be addressed. E-mail: zhangqc@ustc.edu.cn

teraction between dislocation and diffusing solutes is proposed and the results self-consistently exhibit three branches of the dislocation-solute interaction.[14,30]

Precipitate particles, which cause distortion of a lattice, preclude dislocation motion and affect plastic deformation of an alloy, notably influence the plastic instability mechanism of alloys. Most research was focused on glide and forest dislocations and solute clouds, so the effect of precipitates in PLC is still under discussion. The undermentioned experiment procedure is put forward to change the solute concentration and the content of precipitates in Al alloy.

Al–Cu alloy system constitution diagram in Fig.1[31] shows that the solubility of Cu in Al matrix increases with temperature increasing in a certain range and reaches a maximum of 5.65 wt.% at 548 °C. The aluminum alloy used in the present experiment contains 3.8–4.9 wt.% Cu, and not all Cu is dissolved in Al. For instance at 300 °C after sufficient anneal, only 0.45 wt.% Cu dissolves and forms α solid solution, and the rest exists as precipitate. A component of these precipitates is $CuAl_2$ or Al_2CuMg.

However, we can obtain supersaturated solid solution which is temporarily stable at room temperature by solution treatment (ST). When alloys are kept at a certain elevated temperature for some time and quenched in water at room temperature, the solid solution has been frozen before the secondary phase can precipitate. The solute concentration of the solid solution is equal to the solubility limit at ST temperature. With the adoptive ST temperature increasing, solute concentration increases and the quantity of precipitates decreases. So with ST at different temperatures we can vary these two parameters to study their influence on PLC effect.

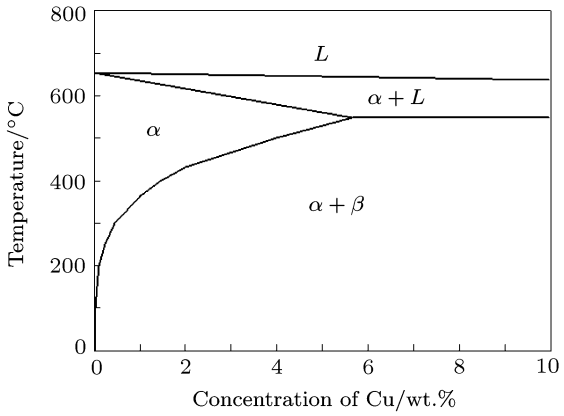


Fig.1. Al–Cu alloy equilibrium phase diagram.

2. Experimental procedure

The referred material is industrial aluminium alloy A2024 and its main chemical compositions in weight percent are given in Table 1. The specimens with a gauge of $50 \times 20 \times 3$ mm^3 were cut from plates along the rolling direction. Before the test, the tensile specimens were kept at 500 °C for 3 h to dissolve solute atoms, viz. Cu and Mg, into Al matrix adequately. And then the specimens were furnace-cooled to the temperatures for solution treatment (ST temperature), i.e. 500, 400, 300, 200 and 100 °C, and kept at ST temperature for 5 h. Finally they were quenched in water.

The tensile tests were performed at room temperature with four different loading speeds: 5, 50, 250 and 500 μm/s, corresponding to nominal strain rates: 10^{-4}, 10^{-3}, 5×10^{-3} and 10^{-2} s^{-1}, respectively. The data of load were recorded at a rate of 100 Hz. At the same time, the DSPI[28,29] a real-time two-dimensional observation method, was used to measure the geometric and kinetic aspects of the PLC deformation bands. With the aid of the DSPI technique, the deformation distribution of the specimen containing PLC deformation bands can be visualized as fringe patterns.

Table 1. Main chemical compositions of Al alloy A2024 (in wt.%).

Cu	Mg	Mn	Si	Fe	others	Al
3.8–4.9	1.2–1.8	0.3–0.9	0.5	0.5	≤ 0.7	balance

The micro-structure of alloys, especially the size and the distribution of precipitates, was examined with the help of a transmission electron microscope (TEM). The specimens were machined into a Φ3 mm circular sheet, and electrolytically thinned in a 4 vol.% alcoholic solution of $HClO_4$. The shin zone with a thickness of 50 μm was observed on a JEOL-2011 TEM. Energy spectrum analysis was used to measure the component of some regions.

Macroscopic and microscopic tests each were completed in 3 h. In the previous work the influence of natural aging (NA) on characteristics of plastic instabilities has been studied. Figure 2[32] shows the serrated stress–time curves for the solution treated samples with different aging durations at an imposed strain rate of 5×10^{-3} s^{-1}. The influence of NA in 3 h could be ignored.

Annealed specimens were brought into comparison in the same tensile tests. These samples were

annealed at 500 °C for 3 h and then slowly cooled to ambient temperature before tension.

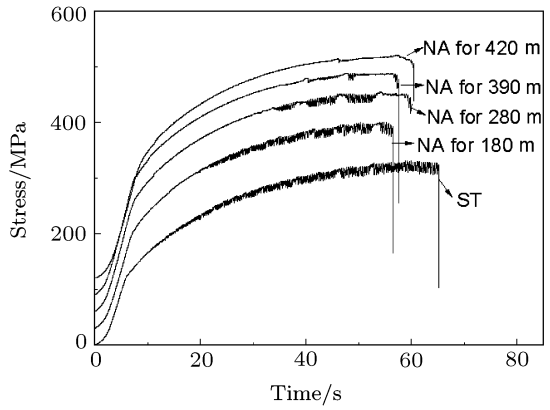


Fig.2. Effect of natural aging on the serrated yielding at an imposed strain rate of 5×10^{-3} s^{-1}. For a better view, each curve is shifted upwards by 30 MPa with respect to the neighbouring one with shorter aging duration.

3. Results

Figure 3 shows the plots of stress versus time for annealed and ST samples at a strain rate of 10^{-4} s^{-1} separately. The stress value of each curve at the same strain changes as a function of ST temperature. It decreases with ST temperature reducing from 500 °C to 300 °C, and then increases appreciably as ST temperature decreases down to 100 °C. The minimum stress corresponds to the annealed specimen. Such an evolution trend is the same as that of tests at other strain rates.

To explore the evolutions of stress drop amplitude and reloading time (refer to the inset in top right corner of Fig.3(b)) with tensile time for different heat-treatment processes, figures 4(b) and 4(c) respectively display their statistical results. Except that both of them increase with plastic deformation for each curve as is known, we can find their non-monotonic dependence on ST temperature. This dependence is shown by the evolutions of average stress drop amplitude and average reloading time with ST temperature in heat-treatment process at several strain intervals in Fig.5. During each strain interval average stress drop amplitude decreases with ST temperature increasing from 100 °C to 300 °C, reaches minimum at 300 °C and then increases with ST temperature until 500 °C. Evolution of average reloading time has a similar trend. These two parameters of annealed samples are close to those of solution-treated samples at 100 °C.

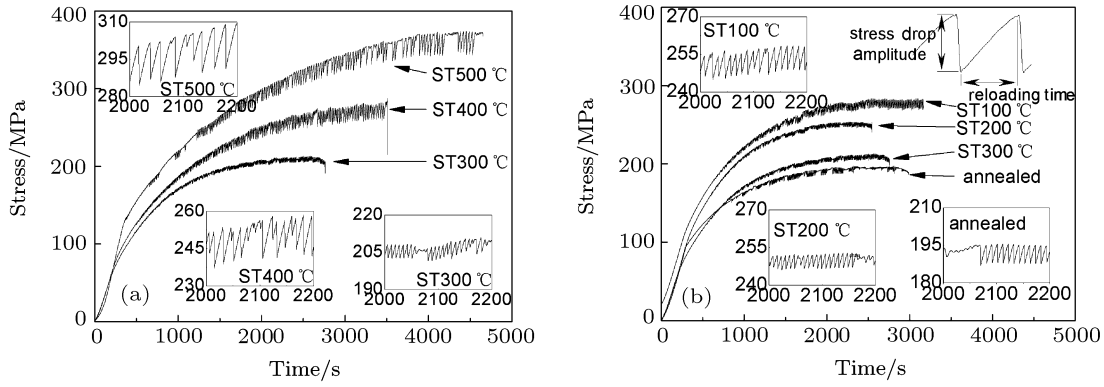


Fig.3. Stress-time curves of A2024 aluminum alloys for different heat treatments at an imposed strain rate of 10^{-4} s^{-1}. The insets show the corresponding amplified fractions of curves between 2000 and 2200 s. The gray curve of ST300 °C in both panel (a) and panel (b) is used for comparison. The curve of ST100 °C in panel (b) is shifted upwards by 20 MPa for a better view.

The dependences of average stress drop amplitude and average reloading time on ST temperature at other imposed strain rates are similar to those in Fig.6, and these curves reach their lowest points at an ST temperature of 300 °C. For the same ST temperature, these two parameters decrease with strain rate increasing. And the variations in amplitude of the reloading time at higher strain rates are higher than those at lower strain rates.

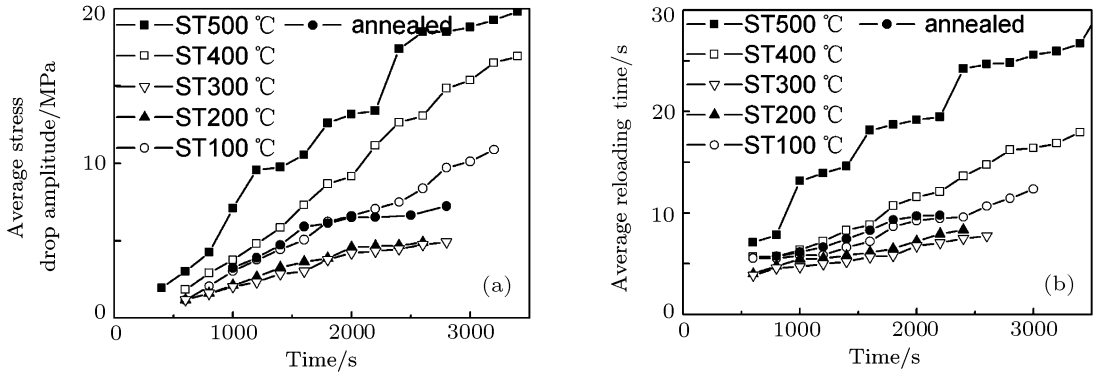


Fig.4. Evolutions of average stress drop amplitude (a) and average reloading time (b) with tensile time for different heat-treatment processes at an imposed strain rate of 10^{-4} s^{-1}.

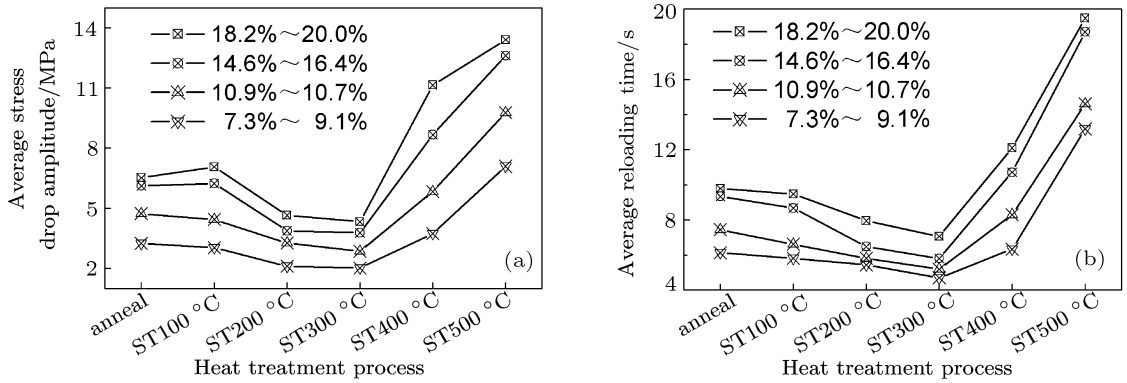


Fig.5. Evolution of (a) average stress drop amplitude and (b) average reloading time with ST temperature in the heat-treatment process at an imposed strain rate of 10^{-4} s^{-1}.

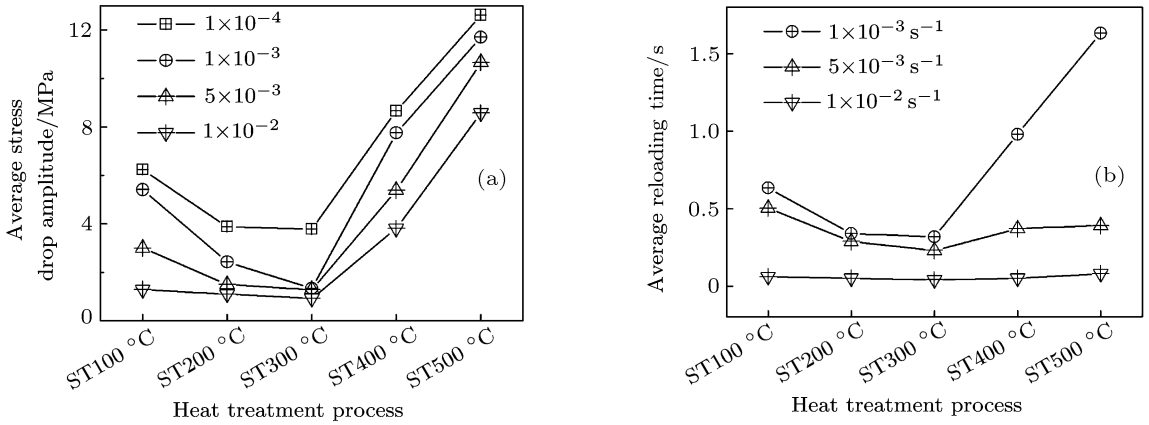


Fig.6. Evolution of average stress drop amplitude (a) and average reloading time (b) with ST temperature in the heat-treatment process at different imposed strain rates in a strain interval of 14.6%–16.4%.

Besides the characteristics of serrated flow of the stress curve, the spatiotemporal evolutions of PLC band after different heat-treatment processes are also studied. Figure 7 shows the plots of band position versus time for annealed and ST samples at a strain rate of 10^{-4} s^{-1}. As reported in other papers,[28,33] the PLC effect in annealed alloys changes from types C to B to A with applied strain rate increasing. Therefore, the representative type A PLC effect, characterized by continuous band propagation as shown in Fig.7(a), is expected in solution-treated alloys at the same imposed strain rate. But, in fact, as shown in Fig.7, the propagation characteristic of bands exhibits two different branches after samples have been solution-treated at different temperatures. When

ST temperature is increased from 100 °C to 300 °C, bands travel along the gauge by hopping just like type B (refer to Figs.7(b), 7(c) and 7(d)). In the tests of ST400 °C and ST500 °C, shear bands nucleate randomly on the sample surface and do not propagate, indicating type C (refer to Figs.7(e) and 7(f)). This phenomenon is coincident with the trend of stress drop amplitude, i.e. the oscillation amplitude of type C serrations is bigger than that of type B.

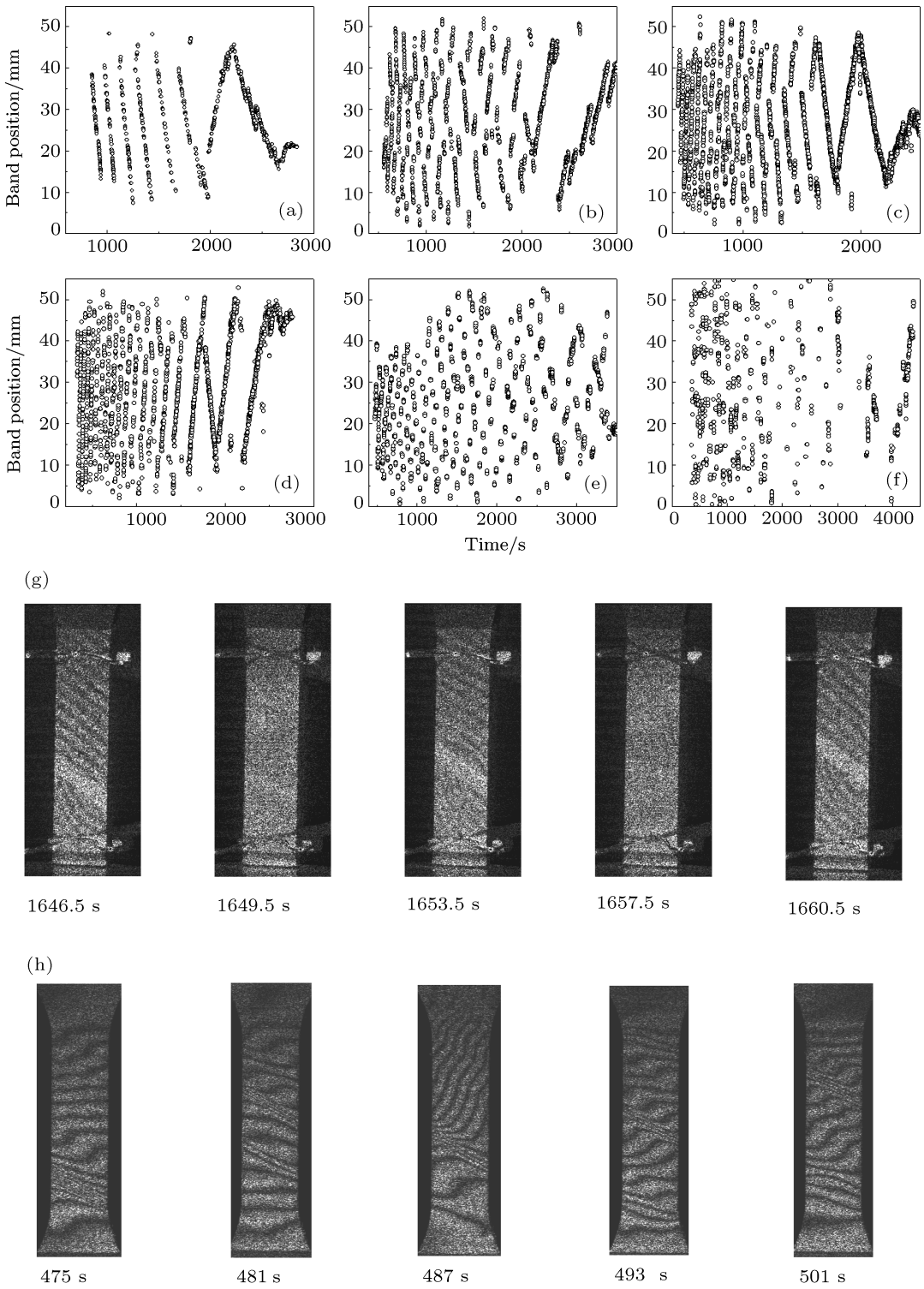


Fig.7. Plots of band position versus time at a strain rate of 10^{-4} s^{-1} for A2024 aluminum alloys with annealing (a), and ST at 100 (b), 200 (c), 300 (d), 400 (e), 500 (f) separately, and images for a series of correlation fringe patterns showing the hopping propagation of type B bands (g) and correlation fringe patterns indicating the stochastic nucleation of type C band (h), where the time marked under each image is the corresponding deformation time.

Figures 7(g) and 7(h) show the correlation fringe patterns representing the kinematical characteristics of these two types of PLC bands, i.e. type-B band discontinuously hops through the specimen (in Fig.7(g)), and type-C band nucleates randomly in the gauge length (in Fig.7(h)). The existence of the "white band" in each pattern is due to the avalanche-like shearing deformation, which makes the fringes too dense to be distinguished.

The spatiotemporal evolution trends about serrated flow and strain localization mentioned above are similar to those at other strain rates but not shown here. What is worth mentioning is that the spatiotemporal characteristic tends to simplex with a different ST temperature at a high strain rate.

The mechanism of the macroscopic test results above is closely related to the micro-structure and solute concentration of alloys, so corresponding microcosmic experiments are necessary. The structure and the distribution of precipitates can be obtained by TEM. Without an available method, the solute concentration in solid solution is determined only by atom solubility and precipitate content. Figure 8 gives the TEM images of the microstructures of samples after three typical heat treatments. We can find the notable influence of ST on the microstructure of alloys, viz. the size and the distribution of precipitates.

In the samples after ST at 500 °C, only some very fine particles can be seen and they distribute sparsely. After ST at 300 °C, the size of precipitate particles is about several nanometers and their spacing in between is large. Acerose and quasi-globular particles are observed. After ST at 100 °C the sizes of precipitate particles range from about 10 nm to 20 nm, and its distribution is rather dense. The accumulation of particles can be observed. It is concluded that the components of these precipitates are $CuAl_2$ or Al_2CuMg by energy spectrum analysis. This trend is consistent with our conjectured one by analysing alloy phase diagram, or rather, precipitate particles in alloys become bigger and denser with ST temperature decreasing.

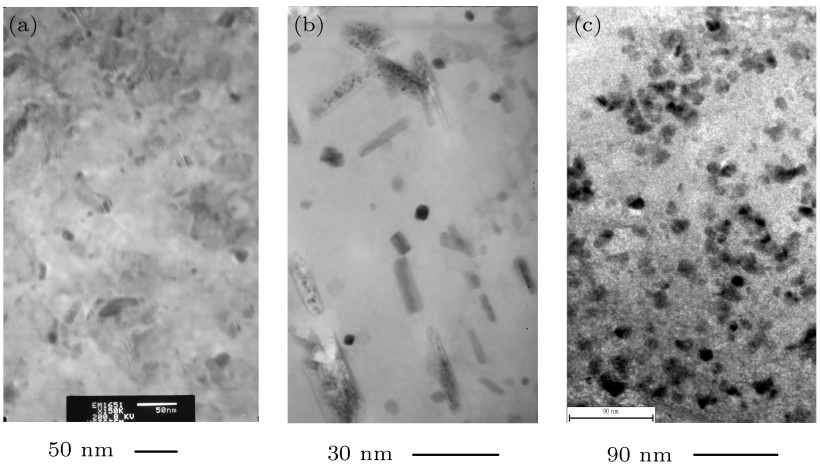


Fig.8. TEM images of precipitates obtained after the heat treatments at 500 °C (a), 300 °C (b) and 100 °C (c).

4. Discussion

According to the conventional DSA model, namely solute-dislocation model, solute concentration on the dislocation lines is determined by solute concentration in bulk besides aging time. Therefore in a more concentrate solid solution glide dislocations are pinned by solute cloud more sufficiently.[14,23−27] The pinning strength increases with ST temperature increasing, and consequently stress drop amplitude and reloading time should increase with ST temperature increasing. But in fact, only when ST temperature is higher than 300 °C, will the evolutions of stress drop amplitude and reloading time accord with this trend.

When ST temperature is lower than 300 °C, coherent precipitates are formed as shown in Fig.8(c),

and content of particles increases with ST temperature decreasing. Coherent precipitates could serve as potential barriers to preclude the dislocation from moving just as other barriers do. Since they are not so easy to overcome as normal short-range barriers (e.g. forest dislocations), a more effective dislocation pile-up will develop after a certain amount of deformation.[34] When a strong enough pile-up stress is built up, the precipitates will be overcome and a large number of dislocations could move collectively through this passage. With ST temperature decreasing, the extent for the dislocation motion to be impeded by precipitates increases. To conquer these potential barriers, glide dislocations must take a longer time to accumulate pile-up stress, so reloading time can also increase with ST temperature. When ST temperature is higher than 300 °C, solute atoms are dissolved adequately and the concentration of solid solution becomes relatively high. On the other hand, precluding fine and sparse precipitate particles from being converted into mobile dislocations can be ignored. Therefore the micro-mechanism of DSA is dominated by solute cloud.

Therefore it is concluded that when solute concentration is relatively high the solute cloud becomes a key factor of DSA; and when plentiful precipitate particles exist they will play a leading role in DSA mechanism. At a certain pivotal point, which is achieved when ST temperature is 300 °C in this paper, these two mechanisms are in equilibrium, i.e. they are coexisting.

As the size of precipitate particles reaches several hundred nanometers, exceeding the action range of solute cloud greatly, spatial coupling behaviour of shearing bands occurs more frequently. Experimental and theoretical studies have proved that spatial coupling leads to a higher spatial correlation of bands.[30] So the propagation characteristic changes from continuous to discrete with ST temperature increasing as shown in Fig.7.

5. Conclusions

In the present article, STs at different temperatures are used to change solute concentration and content of precipitates in Al–Cu alloy, and their operations in DSA effect are discussed. The following conclusions may be drawn from the present study.

(i) Precipitate particles have a remarkable effect on the micro-mechanism of DSA as well as the solute cloud. When solute concentration is relatively high, the solute cloud becomes a key factor of DSA. When plentiful precipitate particles exist, the mechanism of DSA is determined by precipitates.

(ii) In each strain interval the average stress drop amplitude decreases with ST temperature increasing from 100 °C to 300 °C, reaches a minimum at 300 °C and then increases with ST temperature increasing up to 500 °C. Evolution of the average reloading time has a similar trend. These two parameters of annealed samples are close to those of solution-treated sample at 100 °C.

(iii) Precipitates and the solute cloud have an effect on the behaviour of shear bands. A study of tentative explanation, where the effect of spatial coupling on propagation of shearing bands tentative explanation is taken into account, is under way.

References

[1] Le Chatelier M A 1909 *Rev. Metall.* **6** 914

[2] Portevin A and Le Chatelier F 1923 *Comp. Rend. Acad. Sci. Paris* **176** 507

[3] Bell J F 1973 *Encyclopedia of Physics, Mechanics of Solids* I (Berlin: Springer) p41 and p649

[4] Brindley B J and Worthington P J 1970 *Metall. Rev.* **15** 101

[5] Chihab K, Estrin Y and Kubin L P 1987 *Scripta. Metall.* **21** 203

[6] Pink E and Grinberg A 1981 *Mater. Sci. Eng.* **51** 1

[7] McCormick P G 1986 *Trans. Indian. Inst. Met.* **39** 98

[8] Hähner P, Ziegenbein A, Rizzi E and Neuhäuser H 2002 *Phys. Rev.* B **65** 134109

[9] Cottrell A H 1953 *Dislocations and Plastic Flow in Crystals* (Oxford: Oxford University Press)

[10] McCormick P G 1972 *Acta Metall.* **20** 351

[11] Van den Beukel A 1975 *Phys. Status Solidi.* A **30** 197

[12] Lebyodkin M, Brechet Y, Estrin Y and Kubin L 1996 *Acta Mater.* **44** 4531

[13] Hahner P, Zigenbein A, Rizzi E and Neuhauser H 2002 *Phys. Rev.* B **65** 134109

[14] Chen Z J, Zhang Q C and Wu X P 2005 *Europhys. Lett.* **71** 235

[15] Cottrell A H and Bilby B A 1949 *Proc. Phys. Soc. London* A **62** 49

[16] McCormick P G 1972 *Acta Metall.* **20** 351

[17] Mulford R A and Kocks U F 1979 *Acta Metall.* **27** 1125

[18] Springer F and Schwink C 1991 *Scripta Metall.* **25** 2739

[19] Ananthakrishna G and Sahoo D J 1981 *Phys.* D: *Appl. Phys.* **14** 2081
[20] Kubin L P and Estrin Y 1990 *Acta Metall.* **38** 697
[21] Zaiser M, Glazov M, Lalli L A and Richmond O 1999 *Comp. Mater. Sci.* **15** 35
[22] Fressengeas C, Beaudoin A J, Lebyodkin M, Kubin L P and Estrin Y 2005 *Master. Sci. Eng.* A **400** 226
[23] McCormick P G 1988 *Acta Metall.* **36** 3061
[24] Ling C P, Estrin Y and McCormick P G 1994 *Acta Metall.* **42** 1541
[25] Lebyodkin M, Dunin-Barkovskii L, Brechet Y, Estrin Y and Kubin L P 2000 *Acta Metall.* **48** 2529
[26] Hahner P and Rizzi E 2003 *Acta Mater.* **51** 3385
[27] Chen Z J, Zhang Q C, Jiang Z Y, Jiang H F and Wu X P 2004 *J. Mater. Sci. Tech.* **20** 535
[28] Zhang Q C, Jiang Z Y, Jiang H F, Chen Z J and Wu X P 2005 *International Journal of Plasticity* **21** 2150
[29] Xiang G F, Zhang Q C, Liu H W and Wu X P 2007 *Scripta Materialia* **56** 721
[30] Jiang H F, Zhang Q C, Chen X D, Chen Z J, Jiang Z Y, Wu X P and Fan J H 2007 *Acta Mater.* **55** 2219
[31] Porter D A and Easterling K E 1992 *Phase Transfromations in Metals and Alloys* (2nd edition) (CRC Press, ISBN: 0748757414) p291
[32] Jiang H F, Zhang Q C, Wu X P and Fan J H 2006 *Scripta. Mater.* **54** 2041
[33] Chihab K, Estrin Y, Kubin L P and Vergnol J 1987 *Scripta Metall.* **21** 203
[34] Chmelik F, Pink E, Krol J, Balik J, Pesicka J and Lukac P 1998 *Acta Mater.* **46** 4435